Numerical investigation on the fire resistance of load bearing LSF walls: the effect of the load level

Alan Vítor Devens[1,2], Paulo A. G. Piloto[1], Diego R. Rossetto[2]

[1]*Dept. of Applied Mechanics, Instituto Politécnico de Bragança*
Campus Sta. Apolonia, 5300-252, Bragança, Portugal
alandevens@alunos.utfpr.edu.br, ppiloto@ipb.pt
[2]*Dept. of Mechanical Engineering, Universidade Tecnológica Federal do Paraná*
Via do Conhecimento, 85503-390, Paraná, Brazil
diegorossetto@utfpr.edu.br

Abstract. This article investigates the fire performance of Light Steel Frame (LSF) walls commonly used in buildings. Six full-scale LSF tests with different layouts are validated through numerical simulations using uncoupled thermal and mechanical analyses. The hybrid numerical model incorporates experimental data to accurately predict the LSF wall temperature, solving the non-linear transient thermal analysis. Three mechanical simulations are developed: elastic buckling analysis for instability mode, Geometric and Material Non-Linear Imperfection Analysis (GMNIA) for load-bearing capacity at room temperature, and thermo-mechanical analysis considering temperature effects under constant load. Model validation compares six experimental tests under room temperature and fire conditions. The Root Mean Square Error is used for each comparison. Results show that the fire resistance (R) of LSF walls decreases with the load level. The impact of the cavity insulation is examined, revealing potential improvements in fire resistance for cavity-insulated LSF hollow stud walls compared to non-insulated ones. Notably, hollow section studs generally exhibit higher fire resistance than corresponding lipped section studs when void cavities are used. The investigation proposes a new approach to determine the fire resistance based on the relationship between the critical temperature of steel studs (Hot flange) and load levels. This relationship allows us to predict the fire resistance time through a preliminary thermal analysis of LSF walls.

Keywords: LSF walls, load-bearing walls, fire resistance, numerical simulations.

1 Introduction

In recent times, the steel structural system has witnessed a remarkable resurgence, captivating designers and construction contractors seeking cutting-edge technologies. As an advanced alternative to traditional masonry methods, steel construction has become the new standard, offering enhanced benefits from industrialised construction. Within steel construction, the Light Steel Framing (LSF) system has emerged as a prominent player, heralding lighter and more cost-effective steel structures in residential buildings across North America, the United Kingdom, Australia, Japan, and even gaining popularity in emerging economies. While steel structures are favoured for their strength and durability, they face a significant challenge when exposed to high temperatures during fire events. Under such conditions, steel begins to lose strength and stiffness, leading to high deformations and instabilities, potentially resulting in catastrophic hazards. Consequently, it becomes crucial to ensure the fire safety of LSF structures, focusing on minimizing risks to life and property loss.

Addressing these concerns, this investigation introduces a numerical model, validated against six full-scale experiments, to accurately predict the thermo-mechanical behaviour of LSF walls under varying load levels during fire exposure. By establishing a correlation between the load level and the critical temperature, this study offers valuable insights into LSF behaviour in fire scenarios with a new proposal to design LSF walls.

2 Specimens

Structures made by LSF exhibit a distinct assembly pattern. They consist of a steel framework comprising studs and tracks, enclosed by one or more protective plates. This investigation wants to evaluate different types of

assemblies. For that, six experimental fire tests with a similar layout of 3.0x3.0 meters with an arrangement of six studs were spaced every 600 mm from their centres, using standard gypsum as a protective material. A variation of some parameters was selected, such as steel stud grade, and the shape of studs, with and without cavity insulation, as shown in Figure 1. These specimens were selected to evaluate the influence of these parameters on the fire resistance and verify the accuracy of the numerical solution methods.

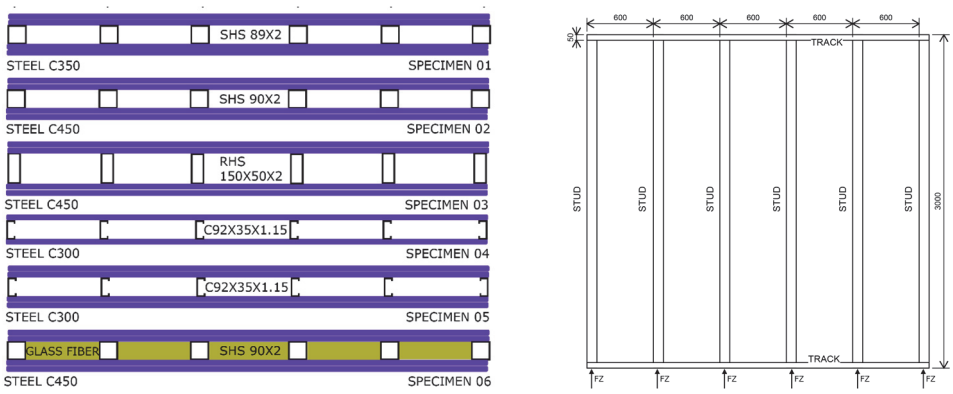

Figure 1. Characteristics of specimens studied.

Specimen 01 is defined in agreement with the experimental investigation developed by Tao et al. [1]. The specimens made of hollow sections 02, 03 and 06 are presented in the work developed by Tao et al. [2], and the specimens 04 and 05, with open shapes, are presented in the work developed by Ariyanayagam and Mahendran [3]. The information on specimens and their results under the fire test is summarised in Table 1.

Table 1. Information on specimens.

ID	STUD SHAPE	STEEL GRADE OF STUDS	NUMBER OF LAYERS	CAVITY	LOAD BEARING [kN]	LOAD LEVEL [%]	FIRE RES. EXP [min]	FIRE RES. NUM [min]
01 [1]	SHS89x2.0	C350	2x16mm	\	187	20	237	↑250
02 [2]	SHS90x2.0	C450	2x16mm	\	193	40	158	141
03 [2]	RHS150x50x2.0	C450	2x16mm	\	182	40	152	↑160
04 [3]	C92x35x1.15	C300	1x16mm	\	40	20	77	↑78
05 [3]	C92x35x1.15	C300	2x16mm	\	40	40	124	↑125
06[2]	SHS90x2.0	C450	2x16mm	Glass fibre	193	40	147	147

3 Mechanical and thermal properties

The thermal conductivity (λ), specific heat (C_p), relative density (ρ) and emissivity (ε) are presented for all the materials involved. Figure 2a presents the thermal properties used for gypsum obtained from the standard prEN1995-1-2 [4]. The thermal properties used for the carbon steel are well established in the EN1993-1-2 [5] (Figure 2b and Figure 2c). The thermal properties used for the glass fibre insulation were obtained from the study developed by Keerthan and Mahendran [6] (Figure 2d). The original density of gypsum consider was 781 kg/m³, 11 kg/m³ to glass fiber, and 7850 kg/m³ to steel. The emissivity was taken as 0.8 for gypsum and 0.7 for steel.

The mechanical properties of four steel grades (C500 used for tracks) followed the Ramberg-Osgood method with a two-stage stress-strain curve scheme developed by Imram et al. [7], using the reduction factors shown in Figure 2d. The properties are determined from the experimental test.

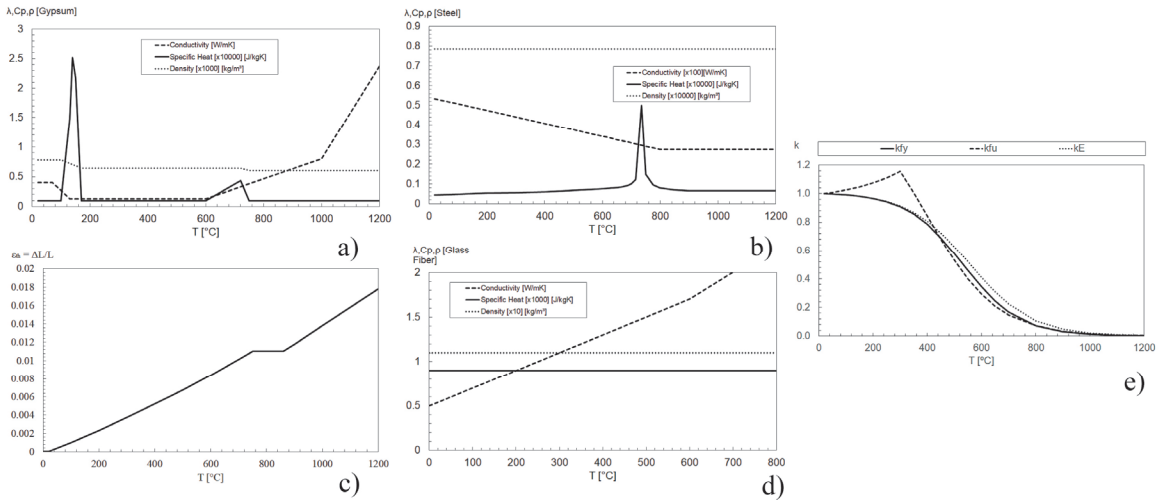

Figure 2. Thermal properties of gypsum (a), steel (b), glass fibre (c), coefficient of thermal expansion of steel (d) and reduction factors to mechanical properties of steel (e).

4 Numerical Validation

4.1 Mechanical model

The finite element "Shell 181" is suitable to model low-thickness elements, and is being used to model the studs and the tracks. The studs were screwed in both extremities (bottom and top) using the tracks made by U-shape, C500 steel grade with 1.95 mm thickness to hollow section stud specimens and 1.15 mm thickness to open section stud specimens. In the physical model, the elements are fixed by screws. To simplify the analysis, joints are modelled by superposition of both steel parts (studs and tracks), using double thickness, sharing the same nodes with in-plane restrain applied to one central node in the horizontal direction (UX=0).

A few additional restrictions were applied to the model. In the top track, the web surface is considered partially restrained, using null displacement in all three directions UX (horizontal), UY (depth), and UZ (vertical) and no rotational restriction. The horizontal restriction (UX=0) is also applied to the screw positions fixing the plasterboard layers to studs. For each stud, the load was distributed by 4 nodes, using the interface beam (web of the track with an extra thickness of 30 mm) to distribute the load over the track and avoid the stress concentration effect. An additional restrain (UY=UX =0) was applied to the central node of the stud, to prevent forces from moving out of the plane.

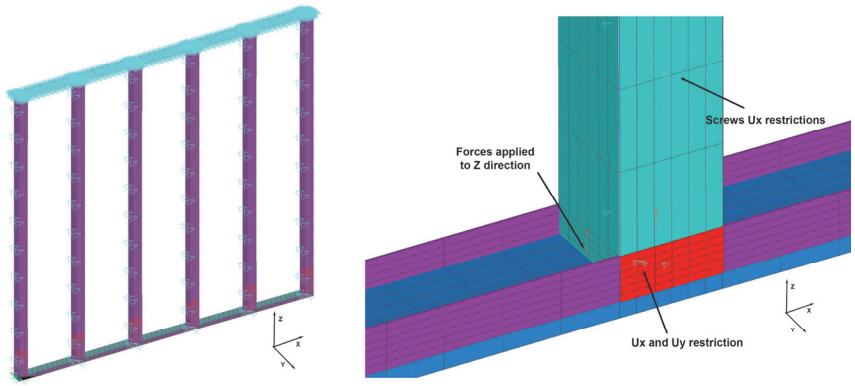

Figure 3. The mechanical model with movement restriction, specimen 01.

An example model and boundary conditions are depicted in Figure 3, where each colour represents a different thickness.

4.2 Imperfections and mechanical model validation at room temperature

The first step is made by a linear elastic buckling analysis at room temperature using the Block Lanczos extraction method to determine the critical load and main instability mode shape of the LSF structure. This instability mode is used to define the imperfection of the structure. A global buckling failure mode was identified for specimens 01, 02 and 06, while a local web buckling failure mode was identified for specimens 03 to 05. The maximum local geometric imperfections in cold-formed steels are given by Schafer and Pekoz [8] and to studs subject to global buckling. A global imperfection with a maximum amplitude of L/1000 has been applied, where L is the buckling length of the stud. With the initial imperfections applied to the geometry, the validation is verified by the load-bearing capacity of specimens at room temperature. The Arc-Length method was used to estimate the load-bearing capacity at room temperature, using the convergence criterion based on displacement with a tolerance of 5% and a reference value of 10^{-3} m. The load increment was defined as 100 [N] with a possible change between 10 and 1000 [N].

Table 2 summarises the results of this section, which may be considered a good agreement between numerical simulations and experimental maximum load. The parametric study is based on a set of load levels, and the load bearing is defined by the numerical results. A maximum difference of approximately 14% was achieved for specimens 02 and 06. However, the authors of the fire tests pointed out the possibility of underestimation in the experimental results, due to some asymmetry in the mounting of the specimens [2].

Table 2. Details of ambient temperature load capacity validation.

ID	MAXIMUM LOAD (EXPERIMENTAL) [KN]	MAXIMUM LOAD (NUMERICAL) [KN]	DIFFERENCE [%]	LOAD BEARING [KN]
01	187	192	2.67	192
02	193	220	13.99	220
03	182	180	-1.10	180
04	40	40	0.00	40
05	40	40	0.00	40
06	193	220	13.99	220

4.3 Thermal model validation

A good thermal model is essential for conducting an accurate and reliable thermomechanical analysis. The hybrid thermal model has been selected based on previous investigations [9]. The same LSF structure models have been defined with additional solid finite elements "Solid 70" to represent the 16 mm external gypsum layers and glass fibre insulation material applied to the cavity. Figure 4a shows the perspective view and a section of the thermal model used for specimen 06. The external layer of gypsum has been removed, see Figure 4b and Figure 4c shows a section view of specimen 06 with the three materials, gypsum (red), glass fibre (dark blue) and steel (light blue). To represent the fire effect on the LSF wall, the convection boundary condition is applied to the fireside surface with a coefficient of 25 W/m²K and bulk temperature evolution with time, following the furnace fire curve from experimental results. The radiation is also applied to the fireside surface with an emissivity equal a 1. In the unexposed surface, only convection is applied, using the coefficient of 9 W/m²K to include the radiation effect, assuming a constant bulk temperature of 20 °C.

This hybrid model also requires the calculation or the definition of the bulk temperature inside the void cavity. For this study, the average temperature measurements between the HF (Hot Flange) and CF (Cold Flange) have been used as bulk temperature, with a convection coefficient of the cavity equal to 17 W/m^{2}K and the flame emissivity equal to 1. For the case of specimen 06 (cavity filled with fibreglass), one decided to apply convection with the same film coefficient (17 W/m^{2}K) and radiation with a reduction in the emissivity to 0.5, inside the hollow section. The thermal validation is verified by the temperature comparison between the numerical and experimental results. The bulk temperature used to simulate convection and radiation on the exposed side was defined by the real furnace curve. Following the standard to fire tests [10] is necessary to apply the standard temperature curve [11], but sometimes the experimental furnace tests present a difference between the furnace curve and ISO 834 curve. A significant difference occurs in specimen 01, where the curves differ by more than 100 °C after 240 min. This difference was explained by the author with a problem in the low-pressure supply of the gas furnace [1].

The thermal solution is transient and nonlinear, using an incremental time step of 60 s, with the possibility to be reduced to 1 s with the time at the end of the simulation equal to the experimental fire test. The convergence

criterion was based on the heat flow, with a tolerance value of 10^{-3} and a reference value of 10^{-6} [W].

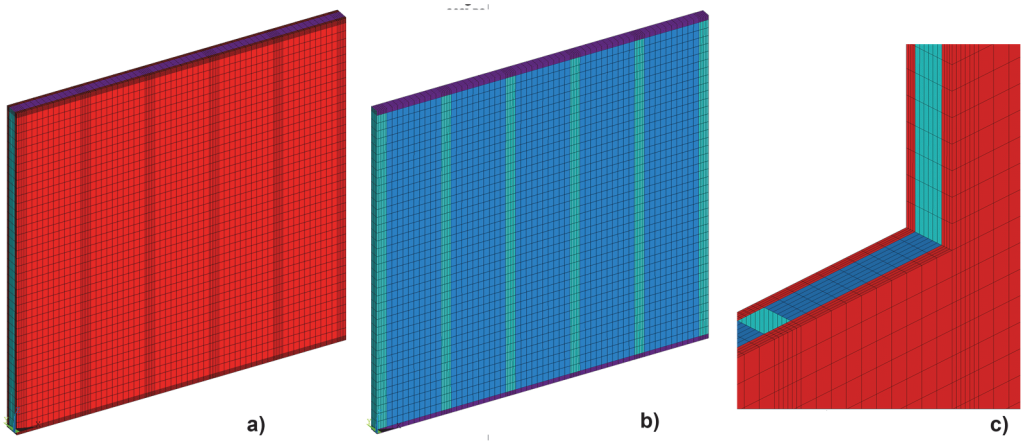

Figure 4. a) External view of the thermal model. b) Omitting gypsum. c) Cut view of specimen 06.

The numerical temperatures are determined by collecting the results over time from nodes closest to the position of the thermocouples, following the same nomenclature. In this paper, to assess the quality of the results, the Root Mean Square Error (RMSE) is applied for the temperature histories of the steel stud, by comparing the finite element analysis and experimental results, every 10 minutes. The results are presented in Table 3, demonstrating an accurate approximation and all specimens. It is worth noting that the recorded temperature by any thermocouple in the furnace shall not deviate from the standard temperature curve by more than 100°C, after the first 10 minutes of any standard fire test, according to EN1363-1 [10].

Table 3. RMSE error for the temperature evolution in all components.

ID	NUMBER OF INSTANTS [N]	RMSE HF [°C]	RMSE CF [°C]	RMSE PB1 [°C]	RMSE PB1-2 [°C]	RMSE PB2 [°C]	RMSE PB3 [°C]	RMSE PB3-4 [°C]	RMSE PB4 [°C]
01	24	75.76	39.99	12.67	102.06	45.04	56.77	25.15	8.75
02	15	47.61	27.93	27.53	124.46	52.14	47.18	13.00	16.08
03	15	36.47	42.70	21.26	109.27	32.97	30.64	9.70	10.52
04	7	20.54	43.59	8.54	-	33.18	32.18	-	23.88
05	12	11.08	19.40	31.77	134.73	39.12	31.03	9.75	10.21
06	15	40.01	57.52	17.37	114.17	111.43	210.62	30.59	24.37

The results of the temperature evolution in PB1-2 show the biggest error and stay above the 100°C of difference by the RMSE. This may have occurred because, in the numerical model, the contact between layers is modelled as perfect, providing a uniform and total heat transfer by conduction. In the fire test, the layers are attached by screws and the position of thermocouples between layers 1 and 2 (PB1-2) can move away from the perfect contact. A similar justification can be drawn to the PB3 temperature of the gypsum plate in contact with the insulation (specimen 06).

4.4 Thermomechanical model validation

To conduct the thermo-mechanical analysis, the model is modified by removing the solid finite elements but their thermal effects are considered from the temperature history. The boundary conditions for displacements remain consistent with those used in the load-bearing simulation, which results in a partially restrained effect within the plane of the wall. With the same load level used in the experimental test, the model undergoes a step-by-step and interactive process for thermo-mechanical analysis. The time step used is initially set to 60 seconds, but it can be decreased to 0.01 seconds if necessary. The Newton-Raphson method is employed, utilizing a convergence criterion based on internal efforts. The force and moment are measured using a reference value of 1 [N] and 1 [Nm] respectively. A tolerance level of 0.1% is considered. All the specimens show a good agreement

regarding the failure mode even if specimens 01, 03, 04, and 05 exhibited non-convergence during the thermal simulation, which coincided with the duration of the experimental tests. Nevertheless, by analyzing the von Mises stress for each specimen, the conclusion can be drawn that a load-bearing failure is expected to be achieved shortly after the respective time, see Table 1.

5 Parametric study

The fire resistance of the models is evaluated by subjecting them to the thermomechanical simulation but with different load levels, ranging from 20% to 80% of the LSF maximum load-bearing capacity at room temperature. with increments of 5%. The same convergence criteria are used for force and moment. The results include time to failure, critical temperature (Hot Flange) and unexposed temperature.

Figure 5a) presents the results obtained from 54 thermomechanical simulations, and Figure 5b) presents a series of 94 experimental and numerical results determined by other researchers ([1]–[3], [9], [12]–[15]), depicting the relationship between the load level and the critical temperature.

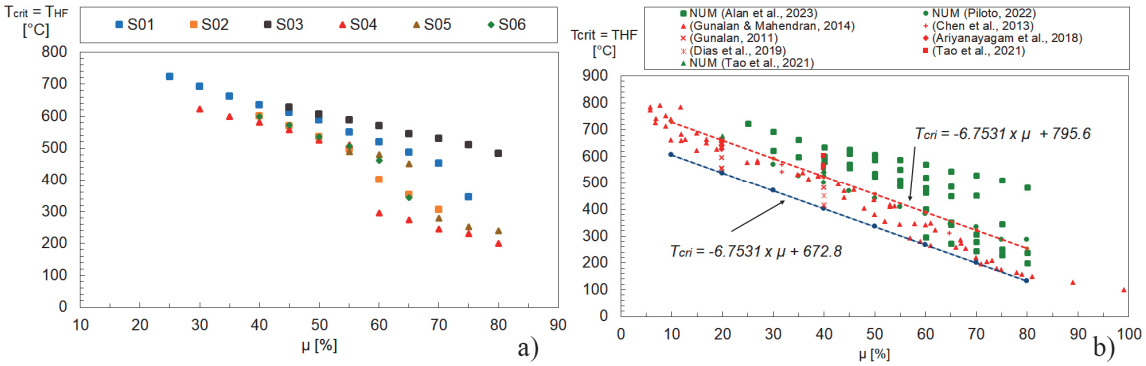

Figure 5. a) Critical temperature of the LSF wall. b) Critical temperature to all LSF structures.

This visual representation allows for a clear understanding of how the critical temperature varies with different load levels. Considering the average value of the HF temperature for each load level, the trendline (red line) and the same trendline minus two times the standard deviation of the numerical results (blue line), a new equation proposal provides a reasonable approximation with a high level of safety (design assisted by testing and simulation). These formulas effectively estimate the critical temperature for all the specimens.

6 Conclusions

The models underwent successful validation of load capacity at room temperature, also exhibited good performance in predicting temperature distribution and the model proved capable of accurately predicting displacements, failure mode and fire resistance (R). Considering the hot flange temperature as the critical temperature for LSF walls, a new equation was proposed to determine the fire resistance based on the results obtained by this investigation and a new compilation of almost a hundred other results from known literature. This proposed relationship enables the prediction of the fire resistance time (R) at a certain load level, through a preliminary thermal analysis of LSF wall types. The results for structures with hollow sections showed a higher critical temperature than those with open sections, which may be a better solution for LSF walls. This is possibly due to the different heat transfer mechanisms of this type of profile. Especially the analysis of the rectangular section which besides showing a higher critical temperature, also showed a lower decrease in FRL with the load level, is probably an excellent stud choice for future applications. Besides the better results regarding the critical temperature, the application of cavity insulation (glass fibre) when using a squared hollow section increased the fire resistance by 5 minutes. This behaviour is not observed in open sections (lipped), which have their fire resistance decreased by the bowing effect. The thickness of the protective layer was studied in specimens 04 and 05, which showed an increase of 4 minutes in fire resistance for each additional 1 mm of gypsum material.

Overall, this investigation provides valuable insights into the fire behaviour of LSF walls with gypsum protection, highlighting the influence of load levels and insulation on their fire performance. The findings contribute to enhancing the design procedure of LSF wall members, promoting improved fire safety standards.

Acknowledgements. Special thanks to the Polytechnic Institute of Bragança for providing the computational tools.

Authorship statement. The authors hereby confirm that they are the sole liable persons responsible for the authorship of this work, and that all material that has been herein included as part of the present paper is either the property (and authorship) of the authors, or has the permission of the owners to be included here.

References

[1] Y. Tao, M. Mahendran, and A. Ariyanayagam, "Load-bearing walls made of cold-formed steel hollow section studs exposed to fire," *Proceedings of 9th International Conference on Steel and Aluminium Structure*, pp. 1533–1544, 2019.

[2] Y. Tao, M. Mahendran, and A. Ariyanayagam, "Fire tests of cold-formed steel walls made of hollow section studs," *J Constr Steel Res*, vol. 178, Mar. 2021, doi: 10.1016/j.jcsr.2020.106495.

[3] A. D. Ariyanayagam and M. Mahendran, "Fire performance of load bearing LSF wall systems made of low strength steel studs," *Thin-Walled Structures*, vol. 130, pp. 487–504, Sep. 2018, doi: 10.1016/j.tws.2018.05.018.

[4] CEN, *prEN 1995-1-2: Eurocode 5 – Design of timber structures*. Brussels: Comité Européen de Normalisation.

[5] CEN, *EN 1993-1-2: Eurocode 3: Design of steel structures - Part 1-2: General rules - Structural fire design*. Brussels: Comité Européen de Normalisation, 2005.

[6] P. Keerthan and M. Mahendran, "Thermal Performance of Composite Panels Under Fire Conditions Using Numerical Studies: Plasterboards, Rockwool, Glass Fibre and Cellulose Insulations," *Fire Technol*, vol. 49, no. 2, pp. 329–356, Apr. 2013, doi: 10.1007/s10694-012-0269-6.

[7] M. Imran, M. Mahendran, and P. Keerthan, "Mechanical properties of cold-formed steel tubular sections at elevated temperatures," *J Constr Steel Res*, vol. 143, pp. 131–147, Apr. 2018, doi: 10.1016/j.jcsr.2017.12.003.

[8] B. W. Schafer and T. Peköz, "Computational modeling of cold-formed steel: characterizing geometric imperfections and residual stresses," *J Constr Steel Res*, vol. 47, pp. 193–210, 1998.

[9] P. A. G. Piloto, M. S. Khetata, and A. B. Ramos-Gavilán, "Analysis of the critical temperature on load bearing LSF walls under fire," *Eng Struct*, vol. 270, Nov. 2022, doi: 10.1016/j.engstruct.2022.114858.

[10] CEN, *EN 1363-1: Fire resistance tests - Part 1: General requirements*. Brussels: Comité Européen de Normalisation, 2020.

[11] ISO, *ISO 834-1 Fire-resistance tests-Elements of building construction-Part 1: General requirements Essai de résistance au feu-Éléments de construction*. Brussels: International Organization for Standardization, 1999.

[12] S. Gunalan and M. Mahendran, "Fire performance of cold-formed steel wall panels and prediction of their fire resistance rating," *Fire Saf J*, vol. 64, pp. 61–80, 2014, doi: 10.1016/j.firesaf.2013.12.003.

[13] S. Gunalan, "Structural Behaviour and Design of Cold-formed Steel Wall Systems under Fire Conditions," Queensland University of Technology, Queensland , 2011. Accessed: Jun. 04, 2023. [Online]. Available: https://eprints.qut.edu.au/49799/

[14] Y. Dias, M. Mahendran, and K. Poologanathan, "Full-scale fire resistance tests of steel and plasterboard sheathed web-stiffened stud walls," *Thin-Walled Structures*, vol. 137, pp. 81–93, Apr. 2019, doi: 10.1016/j.tws.2018.12.027.

[15] W. Chen, J. Ye, Y. Bai, and X. L. Zhao, "Improved fire resistant performance of load bearing cold-formed steel interior and exterior wall systems," *Thin-Walled Structures*, vol. 73, pp. 145–157, 2013, doi: 10.1016/j.tws.2013.07.017.